17. For neurophysiological recording, morphs were six levels of blends of cat and dog (100:0, 80:20, 60:40, 40:60, 20:80, 0:100) and two levels within categories (60:40, 40:60).
18. "Similarity" as defined by the morphing technique and confirmed by an image correlation analysis.
19. Monkeys maintained gaze within 2° of a fixation point throughout the trial. Eye movements were monitored using an eye tracking system (ISCAN, Cambridge, MA). We excluded stimuli that were less than 60% of a given category, as they carried little or no category information. To prevent memorization of sample-test pairs, we chose as the test stimuli a set of 200 randomly generated morphs that were at least 70% of a category. All main effects were observed in both monkeys. For brevity, we summarize their data.
20. This total consisted of 130 neurons from one monkey and 265 from the other. Sample interval activity was summed over 800 ms, beginning 100 ms after stimulus onset. The delay interval activity was summed from 300 ms after sample offset to 100 ms after the end of the delay. Baseline activity was from the 500 ms of fixation before sample onset.
21. T test versus baseline activity, $P < 0.01$. Parametric statistics such as t tests assume normal distributions. Because neuronal activity is sometimes not normally distributed, we also computed nonparametric statistics for all main effects. They yielded a virtually identical pattern of results.
22. T tests on activity from the sample and delay intervals, both $P < 0.001$.
23. $P > 0.6$.
24. Paired t tests between activity of all stimulus-selective neurons in response to the two categories computed in successive 100-ms time bins. A significant difference ($P < 0.01$) began 100 to 200 ms after sample onset, when the earliest PF neurons began responding. The immediate appearance of category information was also evident in average histograms across the neuron population.
25. One-way analysis of variance (ANOVA) on the 54 sample stimuli. Sample interval, 62 neurons; delay interval, 33 neurons; $P < 0.01$.
26. T test that BCD/WCD ratios were significantly different from 1. Sample interval, BCD/WCD mean = 1.30; delay interval, BCD/WCD mean = 1.49; both $P < 0.001$. Category information was significantly stronger during the delay; one-tailed t test, $P = 0.04$. An index of (BCD − WCD)/(BCD + WCD) yielded similar results.
27. Excluding neurons with firing rates below 2 Hz (which produce spurious values when normalized) yielded 55 and 29 neurons with selectivity in the sample and delay intervals, respectively. We normalized each neuron's activity as a proportion of its activity in response to the most effective morph level. To ensure that analyses were not biased toward a category effect, we used only the single stimulus that evoked the maximum response to determine preferred and nonpreferred category.
28. Two-way ANOVA of category membership and level of category (60%, 80%, 100%), test of the category factor. $P < 0.01$ for both intervals.
29. Two-way ANOVA, test of the level factor, $P > 0.6$ for both intervals.
30. ANOVAs on the 27 samples from the preferred or nonpreferred category, either $P < 0.01$.
31. T test on all match versus all nonmatch test stimuli, $P < 0.01$.
32. E. K. Miller, C. A. Erickson, R. Desimone, *J. Neurosci.* **16**, 5154 (1996).
33. T test versus baseline for the sample and/or delay intervals, $P < 0.01$.
34. One-way ANOVA on all 54 samples for the sample and/or delay intervals, $P < 0.01$.
35. Sample interval, mean two-category BCD/WCD = 1.13, t test, $P = 0.22$; delay interval, two-category BCD/WCD mean = 0.96, t test, $P = 0.58$. This analysis was limited to morphs between corresponding cat and dog prototypes (i.e., C1-D1, C2-D2, C3-D3; the vertical morph lines in Fig. 1A) because the other morph lines crossed both the two-category and three-category boundaries. We confirmed that this test could detect two-category information by applying it to the data from the two-category task. The results were virtually identical to the two-category test described above (sample interval, BCD/WCD ratio = 1.33, t test, $P < 0.001$; delay interval, BCD/WCD ratio = 1.57, t test, $P < 0.001$).
36. Three-category BCD/WCD mean = 1.51, t test, $P < 0.01$. As for the two-category test, we compared samples at equivalent distances along between-category morph lines but now using morph lines that crossed the three-category boundaries, but not the two-category boundary. The early appearance of category information in PF activity also suggested that training had altered neuronal selectivity.
37. It was not evident during the sample interval; three-category BCD/WCD mean = 1.03, t test, $P = 0.79$.
38. J. Quintana, J. M. Fuster, *Neuroreport* **3**, 721 (1992).
39. G. Rainer, S. C. Rao, E. K. Miller, *J. Neurosci.* **19**, 5493 (1999).
40. W. F. Asaad, G. Rainer, E. K. Miller, *Neuron* **21**, 1399 (1998).
41. Performance was lower on the three-category task than on the two-category task (87% versus 96%, t test, $P < 0.001$) and reaction times were longer (average 307 ms versus 264 ms, t test, $P < 0.001$).
42. G. Lakoff, *Women, Fire, and Dangerous Things* (Univ. of Chicago Press, Chicago, 1987).
43. R. Dias, T. W. Robbins, A. C. Roberts, *Nature* **380**, 69 (1996).
44. N. P. Bichot, J. D. Schall, K. G. Thompson, *Nature* **381**, 697 (1996).
45. G. Rainer, E. K. Miller, *Neuron* **27**, 179 (2000).
46. I. M. White, S. P. Wise, *Exp. Brain Res.* **126**, 315 (1999).
47. W. F. Asaad, G. Rainer, E. K. Miller, *J. Neurophysiol.* **84**, 451 (2000).
48. M. J. Webster, J. Bachevalier, L. G. Ungerleider, *Cereb. Cortex* **4**, 470 (1994).
49. R. Vogels, *Eur. J. Neurosci.* **11**, 1239 (1999).
50. S. A. Gutnikov, Y. Y. Ma, D. Gaffan, *Eur. J. Neurosci.* **9**, 1524 (1997).
51. G. Rainer, S. C. Rao, E. K. Miller, *J. Neurosci.* **19**, 5493 (1999).
52. H. Tomita, M. Ohbayashi, K. Nakahara, I. Hasegawa, Y. Miyashita, *Nature* **401**, 699 (1999).
53. D. Gaffan, M. J. Eacott, *Exp. Brain. Res.* **105**, 175 (1995).
54. We thank C. Shelton for the morphing software, and K. Anderson, W. Asaad, M. Histed, M. Mehta, J. Wallis, R. Wehby, and M. Wicherski for valuable comments, help, and discussions. Supported by a National Institute of Neurological Disorders and Stroke grant, a NSF Knowledge and Distributed Intelligence grant, the RIKEN-MIT Neuroscience Research Center, a Merck/MIT Fellowship (M.R.), the Whitaker Chair (T.P.), and the Class of 1956 Chair (E.K.M.).

1 September 2000; accepted 15 November 2000

Role of ER Export Signals in Controlling Surface Potassium Channel Numbers

Dzwokai Ma,[1] Noa Zerangue,[1] Yu-Fung Lin,[1] Anthony Collins,[2] Mei Yu,[1] Yuh Nung Jan,[1] Lily Yeh Jan[1]*

Little is known about the identity of endoplasmic reticulum (ER) export signals and how they are used to regulate the number of proteins on the cell surface. Here, we describe two ER export signals that profoundly altered the steady-state distribution of potassium channels and were required for channel localization to the plasma membrane. When transferred to other potassium channels or a G protein–coupled receptor, these ER export signals increased the number of functional proteins on the cell surface. Thus, ER export of membrane proteins is not necessarily limited by folding or assembly, but may be under the control of specific export signals.

Ion channels control neuronal signaling, hormone secretion, cell volume, and salt and water flow across epithelia (*1*). The number of cell surface channels is critical to these physiological functions (*1*). Whether forward-trafficking signals regulate the supply of ion channels to the plasma membrane is not known.

Export from the ER to the Golgi is a key early event in forward traffic. Numerous studies suggest that ER export is limited primarily by quality control (*2, 3*). However, certain secreted and membrane proteins are concentrated in the process of ER export (*4–6*). A motif containing Asp, a variable amino acid, and Glu (DXE) (*7–9*) in vesicular stomatitis virus glycoprotein (VSV-G) has been reported to accelerate the ER export. It is not clear whether ER export signals control the steady-state levels of endogenous membrane proteins destined for later compartments, including the plasma membrane.

The inwardly rectifying potassium (Kir) channels (*10*) Kir1.1 (ROMK1) and Kir2.1 (IRK1) were efficiently expressed in the plasma membrane in *Xenopus* oocytes, whereas several other Kir family members exhibited poor expression or delayed expression kinetics. To test whether these differences correlate with the presence or absence of trafficking signals, we first examined the possible involvement of the variable COOH-termini of these channels (Fig. 1A). Indeed, efficient surface expression (*11*)

[1]Howard Hughes Medical Institute, University of California, San Francisco, San Francisco, CA 94143–0725, USA. [2]College of Pharmacy, Oregon State University, Corvallis, OR 97331–3507, USA

*To whom correspondence should be addressed. E-mail: gkw@itsa.ucsf.edu

was observed when the distal COOH-terminus (amino acids 349 to 428) of Kir2.1 was replaced with that of Kir1.1, Kir2.2 (IRK2), or Kir2.3 (IRK3), but not that of Kir3.1 (GIRK1), Kir3.4 (GIRK4), Kir6.1, or Kir6.2 (Fig. 1B).

To explore the possibility that a forward-trafficking signal resides in the COOH-terminus of Kir2.1, we examined a series of COOH-terminal truncations for their total protein expression, relative surface expression, and channel properties (Fig. 2, A to C). Truncation after residue 374 greatly reduced, but did not eliminate, surface expression, nor did it significantly alter total protein levels (Fig. 2A).

Several lines of evidence indicated that this truncation disrupted forward trafficking rather than channel folding or assembly. First, Kir2.1 (1 to 374) and wild-type channels exhibited identical permeation and rectification properties (*11*). Second, the observed current levels were comparable when normalized to cell surface expression (*11*). Third, wild-type Kir2.1 or truncation mutants Kir2.1 (1 to 374) or Kir2.1 (1 to 385) showed similar single-channel properties [open probabilities (*NPo*) (82.3 ± 6.3%; 79.9 ± 11.3%; 71.9 ± 8.0%), mean open time (in milliseconds) (235.0 ± 115.1; 376.8 ± 10.1; 399.9 ± 28.8), and mean closed time (in milliseconds) (71.2 ± 58.3; 86.0 ± 67.4; 159.7 ± 50.2)] (Fig. 2B) (*11*). Fourth, low surface expression of Kir2.1 (1 to 374) was rescued by coexpression with full-length Kir2.1; this result suggests that the truncated protein can assemble with the wild-type protein (Fig. 2C). Fifth, the COOH-terminal forward-trafficking information of Kir2.1 could be transferred to the NH_2-terminal end of Kir2.1, or to several unrelated proteins (see below). Finally, the trafficking defect of Kir2.1 (1 to 374) was rescued by the fusion of an unrelated 19-residue ER export sequence from Kir1.1 (see below).

To determine whether the forward-trafficking sequences direct Kir2.1 export from the ER, we examined different mammalian cell lines transiently or stably transfected with constructs that encode green fluorescence protein (GFP) fused with wild-type Kir2.1 or COOH-terminal truncation mutants. Like wild-type Kir2.1 (1 to 428), Kir2.1 (1 to 404) and Kir2.1 (1 to 385) resided on the cell membrane and in the Golgi in transiently transfected COS7 cells (Fig. 3A) (*11*). Further truncations left Kir2.1 (1 to 374) and Kir2.1 (1 to 362) primarily in the ER (Fig. 3A); they colocalized with the ER-resident protein BiP and a CD4 fusion protein containing the COOH-terminal KKXX motif for ER retention and retrieval (Fig. 3B) (*11*). The total protein levels of these mutants were comparable to that of wild-type Kir2.1 (*11*). Similar results were observed in NIH 3T3 stable cell lines (Fig. 3, C and D). Thus residues 374 to 385 of Kir2.1 contain a signal important for the ER export.

To define the ER export signal in Kir2.1, we determined the effects of single alanine substitutions of residues from 373 to 385 on the subcellular localization of GFP-Kir2.1 (1 to 385) fusions. Proteins bearing mutations in any of five residues of the FCYENE sequence, including conservative substitutions of acidic residues, lacked detectable plasma membrane localization by GFP fluorescence in most transfected cells (Fig. 3E).

If FCYENE functions as a discrete ER export signal, one would predict that its exact location might not matter as long as it is accessible to the cellular trafficking machinery. Having abolished ER export of GFP-tagged Kir2.1 by mutating FCYENE to FCYANA (Fig. 3F), we inserted residues 369 to 385 of Kir2.1 (which contain FCYENE) either in between GFP and Kir2.1 [GFP-FCYENE-Kir2.1(FCYANA)] or to the COOH-terminus of Kir2.1 [GFP-Kir2.1(FCYANA)-FCYENE]. The resulting fusion proteins were

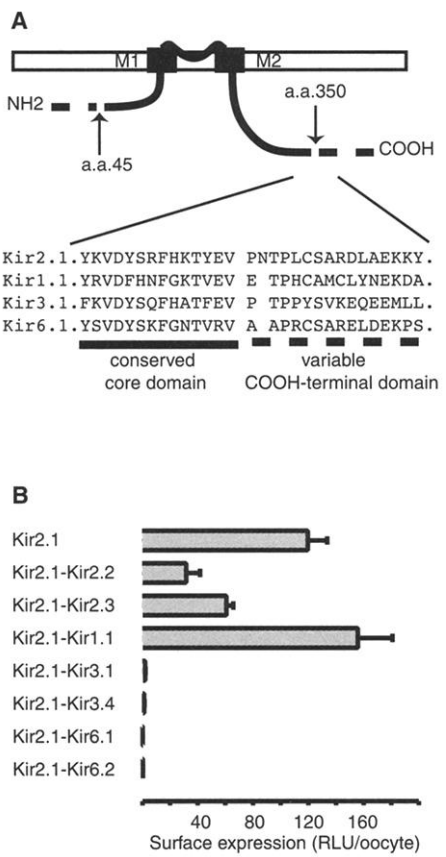

Fig. 1. Kir2.1 surface expression depends on its COOH-terminal sequence. (**A**) Top, topology of Kir channels. Bottom, alignment of sequences that bracket amino acid 350 of Kir2.1, near the border between conserved (represented by the solid line) and variable (represented by the dotted line) sequences. (**B**) Chemiluminescence measurement (*16*) of surface expression in *Xenopus* oocytes. RLU, relative light units.

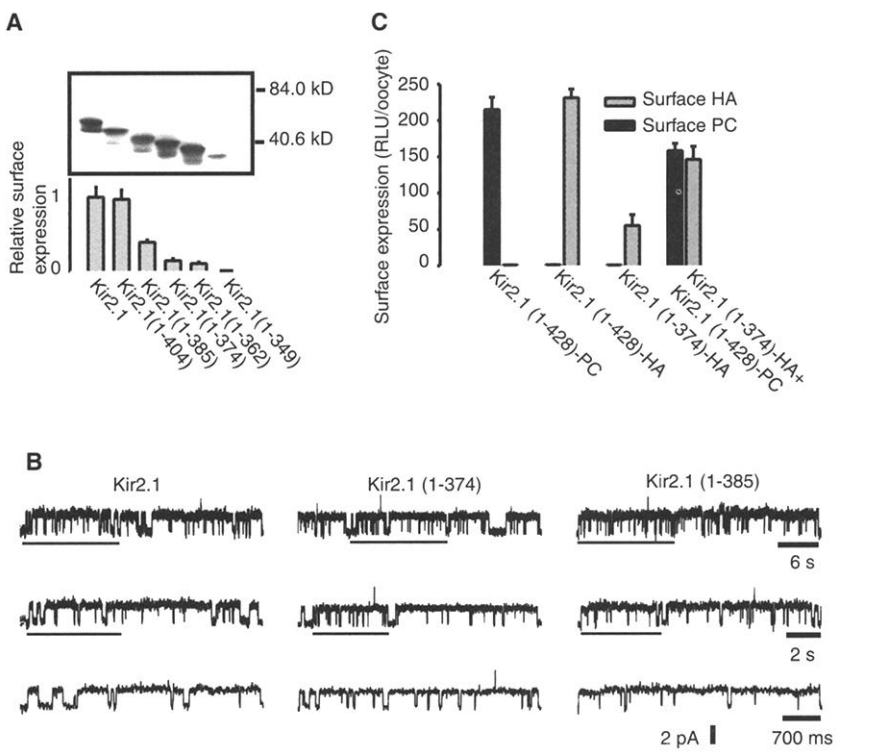

Fig. 2. COOH-terminal deletions greatly reduced the number of Kir2.1 channels on the oocyte surface without affecting total protein levels or channel properties. (**A**) Western blot analysis of total protein and chemiluminescence measurement of surface expression (*16*). (**B**) Representative single-channel current traces (*11*) of Kir2.1 (left), Kir2.1 (1 to 374) (center), and Kir2.1 (1 to 385) (right) channels. Underlined segments of raw traces are shown at increasing temporal resolution (successive traces from top to bottom). Upward deflections represent openings from closed states. (**C**) Single-oocyte surface assays (*16*) indicate coassembly of hemagglutinin (HA)-tagged Kir2.1 and protein C (PC)–tagged Kir2.1 (1 to 374).

efficiently targeted to the cell membrane (Fig. 3F, top), leading to a more than 20-fold increase of surface-expressed channels (Fig. 3F, bottom). Thus, the ability of FCYENE to promote surface expression was largely independent of context.

If FCYENE is a bona fide ER export signal, it would be expected to improve ER export of other membrane proteins. Kir3.1 acquires N-linked endoglycosidase H (endo H)–sensitive core glycosylation at a single Asn residue (Asn^{119}) when expressed alone. This core glycosylation of Kir3.1 is further processed, presumably in the Golgi, to an endo H–resistant form when coexpressed with Kir3.4 (*12*). However, most of Kir3.1 is associated with the cytoskeleton when expressed alone in COS7 cells (*12*). A COOH-terminal truncation mutant, Kir3.1 (1 to 373), localizes to the ER and retains the ability to coassemble with Kir3.4 (*12*). We therefore utilized Kir3.1 (1 to 373) with the hope of monitoring its ER-to-Golgi transport by both immunofluorescence and glycosylation analyses. The addition of FCYENE, but not ACAENE or FCYANA, to the COOH-terminus of Kir3.1 (1 to 373) shifted a significant fraction of proteins from the ER to the Golgi in transfected COS7 cells (Fig. 4A). In pulse-chase studies (*11*), these proteins all remained sensitive to endo H during the 30-min chase period (Fig. 4B). Kir3.1 (1 to 373)-FCYENE but not Kir3.1 (1 to 373), Kir3.1 (1 to 373)-ACAENE, or Kir3.1 (1 to 373)-FCYANA acquired an additional modification that was insensitive to mutations of Asn^{119} and most extracellular Ser or Thr resi-

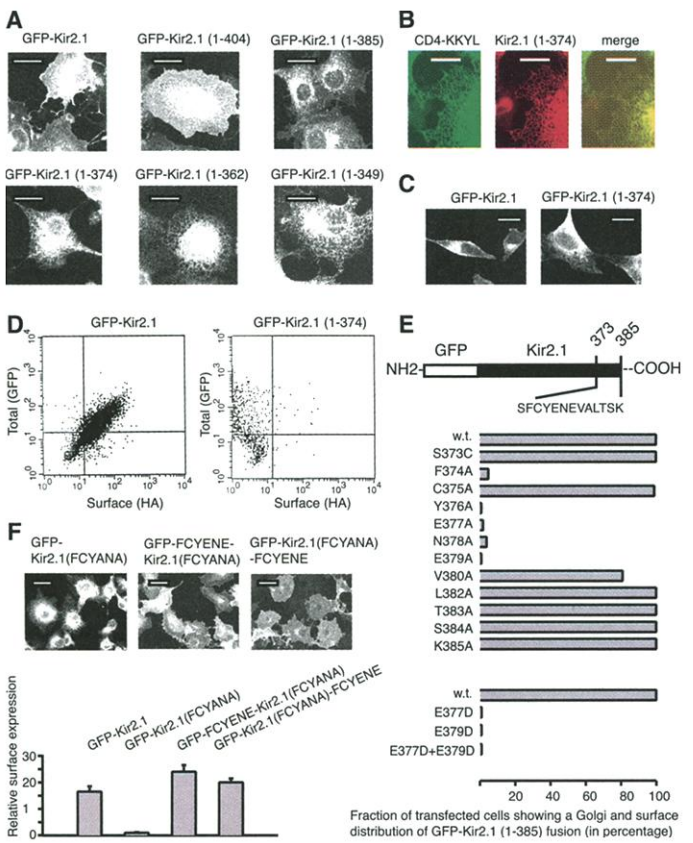

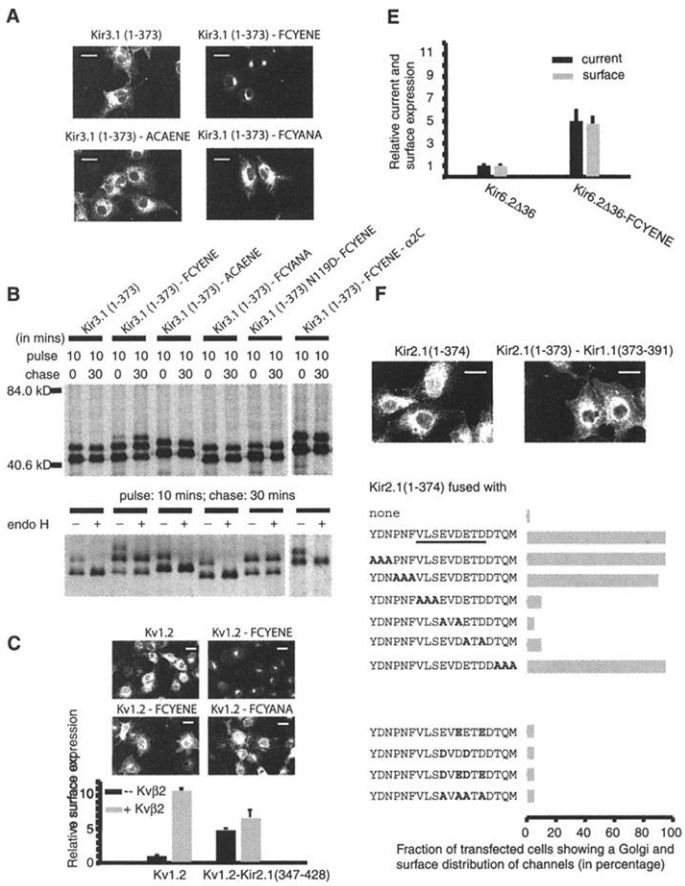

Fig. 3 (left). The FCYENE motif (contained within residues 374 to 385 of Kir2.1) is required for efficient ER export in mammalian cells. (**A**) Subcellular localization of GFP-Kir2.1 fusion proteins expressed in COS7 cells (*11*). Truncating residues before 385 abolishes surface expression. (**B**) Colocalization of Kir2.1 (1 to 374) and CD4-KKYL in the ER (*11*). (**C**) GFP-Kir2.1 but not GFP-Kir2.1 (1 to 374) is present at the plasma membrane in stably transfected NIH 3T3 cells (*11*). (**D**) Flow cytometry analysis of NIH 3T3 cells stably expressing GFP-Kir2.1 or GFP-Kir2.1 (1 to 374) (*11*). The total level of fusion protein was measured by the fluorescence of GFP; surface protein levels were measured by indirect immunofluorescence staining of an extracellular HA epitope. (**E**) Site-directed mutagenesis defines a six–amino acid motif, FCYENE, as critical for the ER export of Kir2.1. (**F**) Immunofluorescence and surface assay for transfected COS7 cells (*15*) reveal that the FCYENE sequence can function at either end of Kir2.1. GFP-Kir2.1 (FCYANA) was generated in pEGFPC1 (*11*) by mutating the FCYENE of Kir2.1 to FCYANA; the mutant fusion protein was retained in the ER. Robust surface expression was observed when residues 369 to 385 (containing a wild-type copy of FCYENE) were inserted either between GFP and Kir2.1 (FCYANA) or onto the COOH-terminus of GFP-Kir2.1 (FCYANA). Scale bars in (A), (C), and (F), 25 μm; scale bars in (B), 10 μm. **Fig. 4 (right).** FCYENE promotes ER export and surface expression of different membrane proteins. Residues 372 to 385 of Kir2.1, which contain FCYENE or the mutated motif ACAENE or FCYANA, were fused to the COOH-termini of test proteins. Experiments were performed in COS7 cells except for Fig. 4E, which was performed in *Xenopus* oocytes. (**A**) FCYENE promotes ER export of Kir3.1 (1 to 373). (**B**) Pulse-chase study [top panel (*11*)] and endo H analysis [bottom panel (*11*)] reveal that FCYENE facilitates the ER export and modification of Kir3.1 (1 to 373). (**C**) Top panel, FCYENE promotes ER export and surface expression of Kv1.2. Kv1.2-FCYENE shows a range of distribution, from the Golgi to the plasma membrane. Bottom panel, promotion of Kv1.2 surface expression by Kvβ2 is mimicked by fusion of FCYENE to Kv1.2. (**D**) FCYENE promotes ER export and surface expression of $GABA_BR1a$-ASRR. (**E**) The addition of FCYENE proportionately increases current and surface protein of Kir6.2Δ36. (**F**) Identification of a distinct ER export signal in Kir1.1. Top panel, fusion of residues 373 to 391 of Kir1.1 to Kir2.1 (1 to 374), which lacks FCYENE and accumulates in the ER, restores the surface expression (*11*). Bottom panel, mutational analysis of residues 373 to 391 of Kir1.1 defines a distinct ER export signal. Introduced mutations are shown in bold type, residues essential for the enhanced ER export are underlined. Scale bars, 25 μm.

dues, as well as neuraminidase and *O*-glycosidase (Fig. 4B). This modification was not observed when Kir3.1 (1 to 373)-FCYENE was retained in the ER by fusing it to the α_{2C}–adrenergic receptor COOH-terminal 14 amino acids (*11*, *13*) (Fig. 4B), containing an RXR(R)-type retention and retrieval motif that could override the ER export signal (see below). Thus channels acquired this modification after exiting the ER, a process promoted by the FCYENE sequence.

The FCYENE sequence exerted a similar trafficking effect on Kv1.2, a voltage-gated potassium channel with little homology to Kir family members (Fig. 4C, top panels). Because coexpression with Kvβ2 improves cell-surface targeting of Kv1.2, Kvβ2 is believed to facilitate the folding and maturation of Kv1.2 in the ER (*14*). Not only did the FCYENE motif mimic Kvβ2 in promoting Kv1.2 surface expression, it also largely occluded the ability of Kvβ2 to further promote surface expression of the fusion protein (Fig. 4C, bottom). Considering the similarity of the effects of Kvβ2 and the FCYENE sequence, it will be interesting to determine whether the ability of Kvβ2 to promote Kv1.2 surface expression reflects improved Kv1.2 folding or the presence of an ER export sequence in Kvβ2.

We next tested whether FCYENE can alter the subcellular localization of proteins that are normally held in the ER by retention and retrieval. We examined Kir6.2 or $GABA_BR1a$ (a subunit of G protein–coupled receptor for the neurotransmitter γ-aminobutyric acid). The latter is a nonchannel protein that exists as a monomer or dimer (*15*). Both proteins, when expressed alone in COS7 cells, remain in the ER via an RXR(R)-mediated retention and retrieval mechanism (*15, 16*). Although deleting RKR from Kir6.2 (Kir6.2Δ36) (*16*) or mutating RSRR in $GABA_BR1a$ to ASRR ($GABA_BR1a$-ASRR) (*15*) resulted in an increase of surface expression, the majority of the protein was still in the ER 24 hours after transfection (Fig. 4D). Strong Golgi staining and further increase of the surface expression were observed when FCYENE was introduced to the COOH-terminus of Kir6.2Δ36 or $GABA_BR1a$-ASRR (Fig. 4D), but not wild-type Kir6.2 or $GABA_BR1a$. FCYENE increased the surface expression and surface currents of Kir6.2Δ36 proportionately (Fig. 4E), suggesting that it did not simply allow misfolded or misassembled channel proteins to escape from the ER. Thus FCYENE could not override the ER retention and retrieval caused by RXR(R) under our experimental conditions. Furthermore, in the absence of RXR(R) retention and retrieval signals, the bulk of Kir6.2Δ36 and $GABA_BR1a$-ASRR exited the ER very slowly, but their ER export could be enhanced by the introduction of an exogenous ER export signal.

The FCYENE motif is conserved in the Kir2 subfamily but is absent in Kir1.1 (*10*), yet the COOH-terminus of Kir1.1 could substitute for that of Kir2.1 in promoting forward trafficking (Fig. 1B). Thus we explored whether the COOH-terminus of Kir1.1 also contained an ER export signal. Indeed, ER export and surface expression were achieved by adding just the last 19 amino acids (YDNPNFVLSEVDETDDTQM) of Kir1.1 to either Kir2.1 (1 to 374) (Fig. 4F, top) or Kir6.2Δ36. Alanine scanning mutagenesis indicated that mutating either of the EXD sequences or the upstream VLS sequence abolished the ER export effect (Fig. 4F, bottom). Furthermore, conservative mutations of the acidic residues (E to D or D to E) were also not tolerated.

Thus, we have shown that Kir1.1 and Kir2.1 contain distinct ER-to-Golgi forward-trafficking signals that do not appear to be required for channel folding, assembly, or gating, but that are essential for export of the channels from the ER. Ion channels such as Kir6.2Δ36 and Kv1.2 largely remain in the ER because of a lack of forward-trafficking signals, and their steady-state surface expression and the current levels can be greatly enhanced by fusion with an exogenous ER export signal. Our results reinforce the notion that signals like the DXE motif of VSV-G increase the ER export rate (*7, 8*), and further demonstrate the physiological significance of diacidic motifs. We have also shown that the flanking residues of diacidic motif are essential for ER export, and they are not limited to Tyr-based residues as previously suggested (*8, 17*). The variation of forward-trafficking signals in different potassium channels presents one potential mechanism for differential regulation of surface channel numbers.

References and Notes

1. B. Hille, *Ionic Channels of Excitable Membranes* (Sinauer Associates, Sunderland, MA, ed. 2, 1992).
2. J. E. Rothman, *Cell* **50**, 521 (1987).
3. S. M. Hurtley, A. Helenius, *Annu. Rev. Cell Biol.* **5**, 277 (1989).
4. M. Mizuno, S. J. Singer, *Proc. Natl. Acad. Sci. U.S.A.* **90**, 5732 (1993).
5. W. E. Balch, J. M. McCaffery, H. Plutner, M. G. Farquhar, *Cell* **76**, 841 (1994).
6. M. J. Kuehn, J. M. Herrmann, R. Schekman, *Nature* **391**, 187 (1998).
7. N. Nishimura, W. E. Balch, *Science* **277**, 556 (1997).
8. C. S. Sevier, O. A. Weisz, M. Davis, C. E. Machamer, *Mol. Biol. Cell* **11**, 13 (2000).
9. Single-letter abbreviations for the amino acid residues are as follows: A, Ala; C, Cys; D, Asp; E, Glu; F, Phe; G, Gly; H, His; I, Ile; K, Lys; L, Leu; M, Met; N, Asn; P, Pro; Q, Gln; R, Arg; S, Ser; T, Thr; V, Val; W, Trp; and Y, Tyr.
10. C. G. Nichols, A. N. Lopatin, *Annu. Rev. Physiol.* **59**, 171 (1997).
11. Supplementary information is available on *Science* Online at www.sciencemag.org/cgi/content/full/291/5502/316/DC1.
12. M. E. Kennedy *et al.*, *J. Biol. Chem.* **274**, 2571 (1999).
13. B. Schwappach, N. Zerangue, Y. N. Jan, L. Y. Jan, *Neuron* **26**, 155 (2000).
14. G. Shi *et al.*, *Neuron* **16**, 843 (1996).
15. M. Margeta-Mitrovic, Y. N. Jan, L. Y. Jan, *Neuron* **27**, 97 (2000).
16. N. Zerangue, B. Schwappach, Y. N. Jan, L. Y. Jan, *Neuron* **22**, 537 (1999).
17. S. I. Bannykh, N. Nishimura, W. E. Balch, *Trends Cell Biol.* **8**, 21 (1998).

18. We thank J. Trimmer for the Kvβ2 cDNA and Y.-M. Chan, M. Margeta-Mitrovic, and other Jan lab members for comments on the manuscript. L.Y.J. and Y.N.J. are Howard Hughes Medical Institute Investigators.

12 October 2000; accepted 5 December 2000

Autoimmune Dilated Cardiomyopathy in PD-1 Receptor–Deficient Mice

Hiroyuki Nishimura,[1] Taku Okazaki,[1] Yoshimasa Tanaka,[2] Kazuki Nakatani,[6] Masatake Hara,[3] Akira Matsumori,[3] Shigetake Sasayama,[3] Akira Mizoguchi,[4] Hiroshi Hiai,[5] Nagahiro Minato,[2] Tasuku Honjo[1]*

Dilated cardiomyopathy is a severe pathology of the heart with poorly understood etiology. Disruption of the gene encoding the negative immunoregulatory receptor PD-1 in BALB/c mice, but not in BALB/c RAG-2$^{-/-}$ mice, caused dilated cardiomyopathy with severely impaired contraction and sudden death by congestive heart failure. Affected hearts showed diffuse deposition of immunoglobulin G (IgG) on the surface of cardiomyocytes. All of the affected PD-1$^{-/-}$ mice exhibited high-titer circulating IgG autoantibodies reactive to a 33-kilodalton protein expressed specifically on the surface of cardiomyocytes. These results indicate that PD-1 may be an important factor contributing to the prevention of autoimmune diseases.

Dilated cardiomyopathy is a chronic disorder of the heart muscle characterized by a poorly contractile and dilated ventricle. The diagnosis is based primarily on clinical criteria and on the exclusion of identifiable underlying causes (*1*). Consequently, patients with dilat-